CPHT Centre de Physique Théorique

# STUDY OF FORWARD DI-JETS IN PROTON-NUCLEUS COLLISIONS IN THE COLOR GLASS CONDENSATE FRAMEWORK

## Supervised by Cyrille Marquet

Ahmed Chahlaoui


INSTITUT
POLYTECHNIQUE
DE PARIS

# ABSTRACT

In high-energy collisions, protons and nuclei are effectively described by quantum states that are densely filled with a significant number of gluons. This condition facilitates a dynamic equilibrium where the emission of new gluons and their nonlinear interactions balance out, leading to a stabilization of gluon densities as they approach a theoretical saturation limit. This phenomenon is the foundational concept behind gluon saturation. The Color Glass Condensate (CGC) effective theory stands at the forefront of our understanding of strongly interacting systems within this saturation regime, offering predictions that can be experimentally verified at high-energy particle colliders. One of the notable forecasts from CGC theory is the vanishing of the away-side peak in the two-particle correlation function during dilute-dense collisions, such as those observed in proton-nucleus interactions in the proton's fragmentation zone (forward rapidity). In this specific setting, due to the saturation effects within the target nuclei, pairs of particles are more inclined to be emitted with a relative azimuthal angle of $\Delta\phi = \pi$ in proton-proton scattering compared to proton-nucleus scattering. This fraction is referred to as the nuclear modification factor. In this project, we aim to reproduce the result of the suppression of this factor in back to back jets. We introduce first the Quantum Chromodynamics (QCD) context before elaborating the role of high energy collisions to our end. Afterwards, we resolve the Balitsky Kovchekov equation (BK) central to this project. This will help us compute the gluons Transverse Momentum Dependent (TMD) distribution, and finally the nuclear modification factor in the CGC framework.

# TABLE DES MATIÈRES

# 1
# INTRODUCTION

The **Standard Model (SM)** of particle physics has garnered multiple successes in discovering and describing quantum phenomena and their effects on particles. This model encompasses three fundamental forces : the strong, the weak and the electromagnetic forces. In this article, we will be focusing on a phenomenon relating only to the strong force and thus a subject of study of the theory of **Quantum Chromodynamics** (QCD).

The strong force was thought to be governing only the interactions between nucleons. However, it was discovered that this effect is only a residual one. The strong force acts mainly on particles inside the nucleons that carry color charges : red, green and blue. These particles are part of a family baptized **quarks** by Murray Gell-Mann. The nucleons are not elementary particles but are composed of three quarks and are types of what we call **hadrons**. But that is not the end of the story. The SLAC experiment has shown that hadrons are made of indeed made of these quarks, which are called valence quarks, but are also submerged in a sea of virtual gluons, the carriers of strong force, and virtual quarks and antiquarks.

This discovery was made possible by the means of **Deep Inelastic Scattering (DIS)**, an experiment that involves the collision of a high-energy electron (or muon) beam with a target nucleon. The process can be viewed as the electron scattering off the quarks inside the nucleon. The interaction is mediated by the exchange of a virtual photon ($\gamma^*$) between the lepton (electron or muon) and a quark within the nucleon as depicted in Fig. 1. The energy and momentum transfer from the lepton to the nucleon (or more precisely, to the quarks inside the nucleon) are high enough to break the nucleon apart, hence the term *deep* (indicating high energy) and *inelastic* (indicating that the target particle is broken apart). The scattered electron and the resulting particles from the disintegration of the nucleon are detected, and their energies and angles of scatter are measured.

The DIS process is parameterized by two important scaling variables (refer to Fig. 1) :

— **Virtuality of the photon** $Q^2 = -q^2 = -(k-k')^2 > 0$. [1] It is a measure of the resolution of the probe ; higher $Q^2$ means finer resolution ($1/Q$).
— **Bjorken-x** : $x = \frac{Q^2}{2p.q}$. It is a dimensionless variable between 0 and 1 which depicts the fraction of the nucleon's momentum carried by the struck quark.

1. The norm is the Minkowskian norm $q^2 = (q^0)^2 - \vec{q}^2$

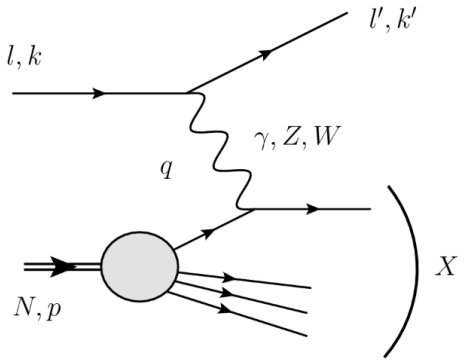


Figure 1 – Feynman diagram representing deep inelastic scattering of a lepton (l) of 4-momentum $k$ on a Nucleon of 4-momentum $p$, at leading order in perturbative expansion. The virtual photon $\gamma$, or a virtual $Z$ or $W$ boson, of 4-momentum $q$ knocks a quark out of the nucleon.

We've mentioned that the virtual photon serves as a probe to the internal structure of the nucleon. It actually interacts with not only the valence quarks but also the sea of quarks and antiquarks. This helps us define a probabilistic chart for the momentum transfer carried by each constituent. For a resolving probe of $Q^2 = 10GeV^2$, the Fig. 2 gives the probability density functions for the partons inside the proton. These are called **Parton Density Functions (PDFs)**. It is worthwhile to remark that at high $x$, the PDFs for $u$ and $d$ dominate. This is mainly because the proton is made of 2 $u$ quarks and 1 $d$ quark. At high $x$, the valence quarks tend to possess most of the momentum transferred. As $x$ gets lower, we remark the apparition of new quark or anti-quarks flavors which are not valence quarks. And starting from the value $x = 0.01$ and lower, the distribution of gluons dominate.[2] This region of low-x values will be the subject of our study, in which the phenomenon of **Gluon Saturation** will emerge.

In order to understand deeply the phenomenon GS, let's look at the type of interactions governed by QCD. The lagrangian of QCD is written as

$$\mathcal{L}_{\text{QCD}} = -\frac{1}{4} G^a_{\mu\nu} G^{\mu\nu}_a + \sum_f \bar{\psi}_f (i\gamma^\mu D_\mu - m_f)\psi_f \tag{1}$$

where

— $G^a_{\mu\nu}$ is the gluon field strength tensor, defined by $G^a_{\mu\nu} = \partial_\mu A^a_\nu - \partial_\nu A^a_\mu + g f^{abc} A^b_\mu A^c_\nu$, with $A^a_\mu$ being the gluon field, $g$ the strong coupling constant, and $f^{abc}$ the structure constants of the SU(3) gauge group.
— $\psi_f$ represents the quark field for a flavor $f$, with the sum running over all quark flavors.
— $\gamma^\mu$ are the Dirac matrices.
— $D_\mu = \partial_\mu + igA^a_\mu T^a$ is the covariant derivative, with $T^a$ being the generators of the SU(3) group in the fundamental representation.
— $m_f$ is the mass of the quark of flavor $f$.

2. The curve is made for $g/10$ and not $g$ in order to fit in the plot.

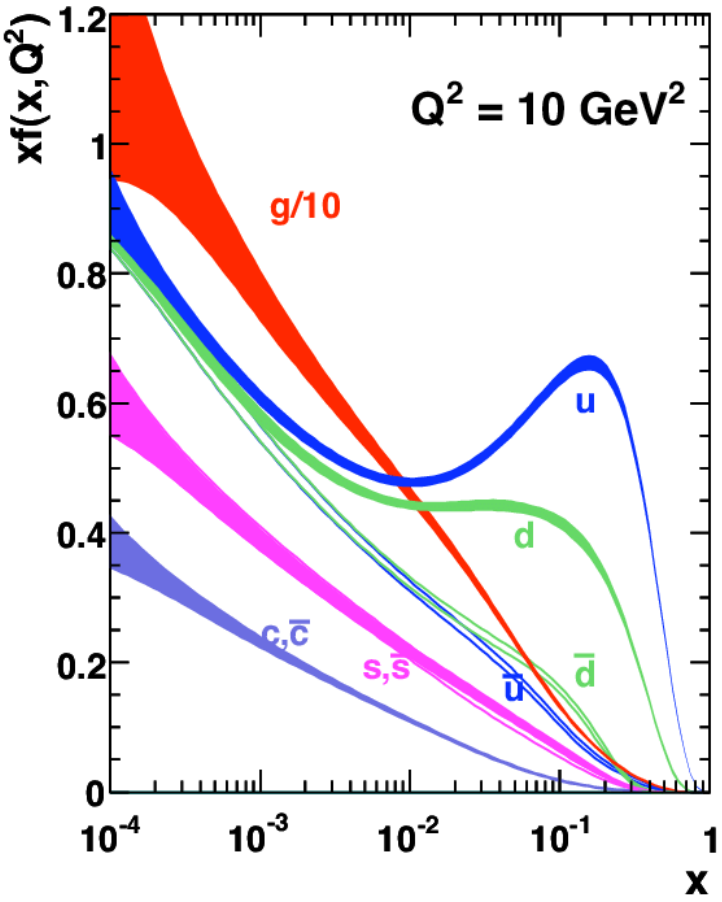


Figure 2 – (PDFs) for the proton's partons at a fixed resolving power of the probe, $Q^2 = 10GeV^2$, as obtained from the MSTW 2008 fits.

The Lagrangian in Eq. 1 depicts the interaction between the gluon fields and the quark fields. Our interest will only lie in the the first term of the Lagrangian. In fact, this term alone describes the self-interacting field of gluons. By containing products of 3 and 4 fields at the same point, it shows the ability of 3 or 4 gluons to interact. [3] This self-interactions leads the over-complexification of the processes at low x regions. Since one gluon can separate into two gluons and these can recombine to form another gluon.

In the low-x regime and thus high energies, we would witness the multiplication of gluons. This is due to the splitting process where a gluon can split into two gluons, and this process is enhanced at small x. Because the gluons are bosons, there's no Pauli exclusion principle to limit their number, so their density can grow very large as the energy of the system increases.

3. This property of self-interacting is proper to all gauge theories with non-commutative gauge groups. Remark that Quantum Electrodynamics (QED) has a gauge group $U(1)$ which is commutative; thus at least three photons don't interact at the same point, otherwise the photon would have charge.

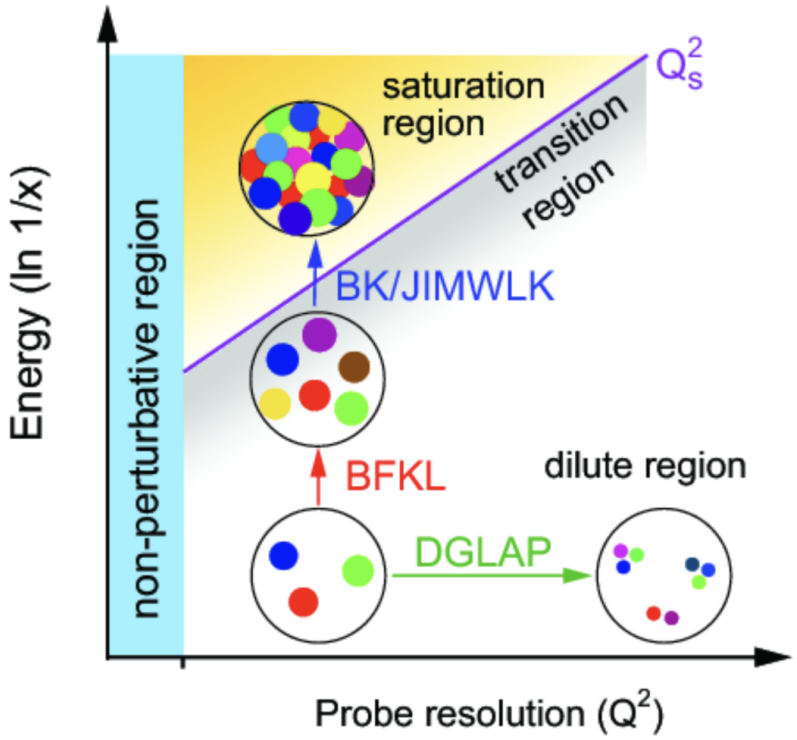


Figure 3 – Evolution of the gluon density in the plane $Q^2$ vs $y = -\ln(x)$

However, there is a physical limit to this growth. As the density of gluons within a given area increases, gluons start to overlap and recombine, effectively taming the growth. This is **gluon saturation** [5]. The gluon density becomes saturated and enters a new regime characterized by non-linear effects described by the BK equation as depicted in Fig. 3

The saturation regime is characterized by a momentum scale called the saturation scale $Q_s$ which depends on the Bjorken variable x. It's a dynamically generated scale that depends on the gluon density and grows with the energy of the collision or the size of the nucleus. At scales below $Q_s$, the gluon density is so high that the addition of more gluons does not significantly change the cross-sections for processes involving those gluons ; the gluon distribution becomes saturated. This regime is effectively studied within the framework of **Color Glass Condensate** which we'll elaborate in section 2.

# 2
# HIGH ENERGY COLLISIONS IN QCD

In this chapter we will elaborate the context of study of our project. First we will introduce collisions in High energy QCD and the kinematic variables used. Afterwards we will elaborate on the case of dilute-dense collisions before detailing the Color Glass Condensate framework.

## 2.1 BOOM : Collisions

A collision between two hadrons is not a bump of two particles like we imagine classically, it is much more abstract than this. A collision between two hadrons is actually an interaction between the quarks and gluons that make them. Way before the collision, or asymptotically, the hadrons are said to be *naked* since they are made only from the valence quarks (the three lines from particles in Fig. 4). Near the collisions, the hadrons become *dressed*, in the sense that their valence quarks are accompanied by virtual quarks-antiquarks pairs and gluons sprung from the hadrons that can be seen in the same figure too. It is worthy of note that this picture is only available in the **perturbative** case, where $\alpha_s$, the strong coupling constant present in the correlation calculations, is too small, i.e $\alpha_s << 1$. However, it is not really a constant, but is a function of the scale of energies $p^0$ of particles present in the process. If $p^0 >> \Lambda_{QCD}$, where $\Lambda_{QCD}$ is the **QCD perturbative scale** and is roughly equals 200 MeV, then we can make perturbative calculations. However, if the energies are of the order of $\Lambda_{QCD}$, then perturbation fails to provide us with precise predictions since $\alpha_s(p^0 \leq \lambda_{QCD}) \geq 1$.

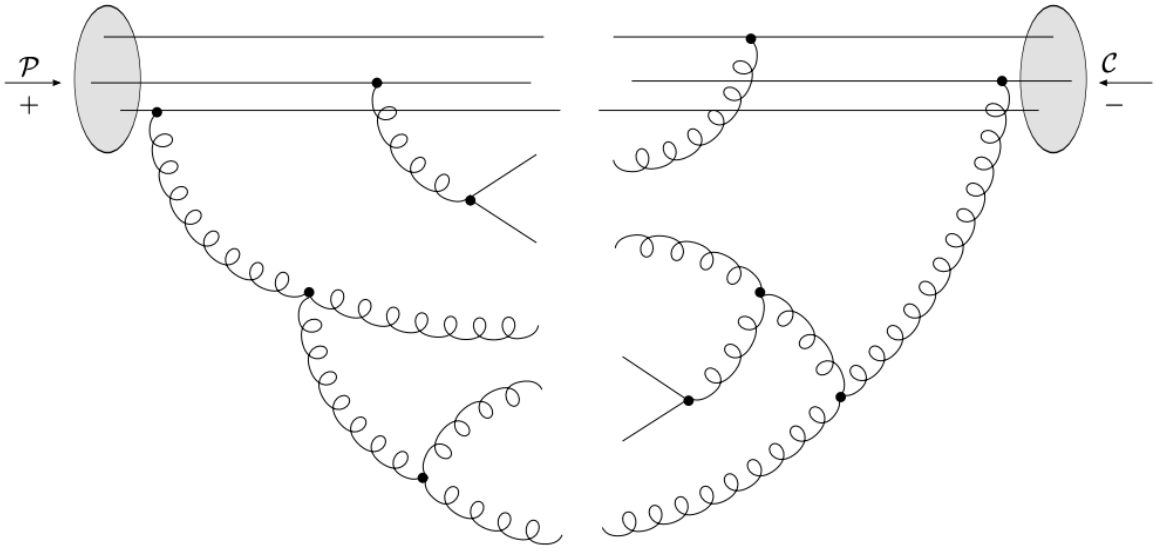


Figure 4 – Collision between a dressed projectile $\mathcal{P}$ and a dressed target $\mathcal{C}$ (cible in french).

A collision between protons for example can produce countless particles. Because of the **confinement** postulate of QCD, quarks and gluons cannot exist freely. They form pairs of quarks and antiquarks from their kinetic energy and thus **hadronize** producing some narrow cones of particles called **jets**. We will be interested in the study of collisions

$$p(p_p) \ + \ A(p_A) \longrightarrow j_1(p_1) \ + \ j_2(p_2) \ + \ X(p_X), \tag{2}$$

where $p$ is a proton, $A$ a nucleus which can be also a proton, $j_i$ are the leading jets, and $X$ is a random set of particles which we will not study. Each particle is accompanied by its 4-momentum labeled $p_*$. These types of collisions are called **di-jet** collisions.

In collisions of two massive particles such as this one, we can artificially label one of them a projectile $\mathcal{P}$ and the other a target $\mathcal{C}$. The experiments in LHC for example are accelerating both particles in a certain center-of mass energy. however, we can position our frame of reference of a the target which will be stationary in this frame. In order to describe the kinematics of such collisions we will introduce the light cone coordinates.

## 2.2 Light Cone coordinates

An event in relativity is linked to point in the space-time defined by $(ct, x, y, z)$. In the metric signature $(+,-,-,-)$, the interval $ds^2$ in Minkowski space is given by

$$ds^2 = c^2dt^2 - (dx^2 + dy^2 + dz^2), \tag{3}$$

where $c$ is the speed of light, $t$ represents time, and $x$, $y$, $z$ are the spatial coordinates.

To simplify calculations, especially in the study of relativistic systems, we can introduce the so-called **light cone coordinates**. These coordinates are defined as :

$$\begin{aligned} x^+ &= \frac{1}{\sqrt{2}}(ct + z), \\ x^- &= \frac{1}{\sqrt{2}}(ct - z), \\ \vec{x}_\perp &= (x, y), \end{aligned}$$

where $x^+$ is referred to as the light cone time, $x^-$ as the light cone space, and $\vec{x}_\perp$ represents the transverse coordinates. Since the the 4-momentum is just the mass of the particle multiplied by derivative of the 4-position by the proper time, these notations can be adopted for 4-momentum too to describe the kinematics. Thus we will use the formula

$$p = (p^0, p^x, p^y, p^z) = (p^+, \vec{p}^\perp, p^-). \tag{4}$$

Another important variable to characterize particles ejected from collisions is the rapidity $y$ defined as

$$e^y = \left(\frac{p^+}{p^-}\right)^{\frac{1}{2}} \tag{5}$$

This variable encodes the angle of the trajectory of the particle with respect to the transverse plane. For example, if $y = 0$, then the ejected particle is in the transverse plane, and the bigger $y$ can get, the further the particle it is from the mentioned plane.

## 2.3 Dilute-dense collisions

Getting back into our collision in Eq.(2), we will denote where $s$ is the squared center of mass energy of the $p + A$ system. It is simply

$$s = (p_p + p_A)^2$$

Since the protons and nuclei are accelerated to an ultra-relativistic speed, they can be considered on the light cone. This makes some simplifications

$$p_p = \sqrt{\frac{s}{2}}(1, 0_t, 0), \quad p_A = \sqrt{\frac{s}{2}}(0, 0_t, 1), \tag{6}$$

The energy (or longitudinal momenta) fractions of the incoming parton (either a quark or gluon) from the projectile, $x_p$, and the gluon from the target, $x_A$, can be expressed in terms of the rapidities and transverse momenta of the produced jets as

$$x_p = \frac{p_1^+ + p_2^+}{p_p^+} = \frac{1}{\sqrt{s}}(|\vec{p_{1t}}|e^{y_1} + |\vec{p_{2t}}|e^{y_2}), \tag{7a}$$

$$x_A = \frac{p_1^- + p_2^-}{p_A^-} = \frac{1}{\sqrt{s}}(|\vec{p_{1t}}|e^{-y_1} + |\vec{p_{2t}}|e^{-y_2}), \tag{7b}$$

where $\vec{p}_{1t}, \vec{p}_{2t}$ are transverse two-vectors of the jets, and $y_1$ and $y_2$ their respective rapidities. By looking at jets produced in the forward direction, we effectively select those fractions to be $x_p \sim 1$ and $x_A \ll 1$. The high momentum coming from the projectile dominates the effect, leading the jets to be going in the same direction as his, thus in the region $y > 0$. This region is called the **forward region**. Since the target $A$ is probed at low $x_A$, the dominant contributions come from the sub processes in which the incoming parton on the target side is a gluon

$$qg \to qg, \quad gg \to q\bar{q}, \quad gg \to gg. \tag{8}$$

These processes will be described by some gluon distributions in the section 4.

In these collisions, entitled **dilute-dense collisions**, the large-$x$ partons of the dilute projectile are described in terms of the usual parton distribution functions of collinear factorization $f_{a/p}$. Whereas, the small-$x$ gluons of the dense target nucleus are described by a transverse-momentum-dependent distribution, which evolve towards small $x$ according to a non-linear equation called the **BK equation**, of which the resolution is a central part of this project and shall be detailed in section 3. Moreover, the momentum $\vec{k}$ of the incoming gluon from the

target, besides the longitudinal component $k^- = x_2\sqrt{s}/2$, has in general a non-zero transverse component, $\vec{k}_T$, which leads to imbalance of transverse momentum of the produced jets

$$|\vec{k}_T|^2 = |\vec{p}_{1t} + \vec{p}_{2t}|^2 = |\vec{p}_{1t}|^2 + |\vec{p}_{2t}|^2 + 2|\vec{p}_{1t}||\vec{p}_{2t}| \cos \Delta\phi, \tag{9}$$

where $\Delta\phi$ is the angle between the two transverse momenta. The fact that $k_T$ is non zero in these processes is a key to component of this study and they cannot be integrated as in the pdfs.

## 2.4 the Color Glass Condensate framework

**The Color Glass Condensate (CGC)** is a state of matter, which is theorized to describe the gluonic content of a hadron, such as a proton or neutron, at high energies. This state is characterized by a high density of gluons, i.e a great number of occupancy in gluons, which are "frozen" in time due to Lorentz time dilation at energies reached in relativistic heavy-ion collisions, thus the introduction of 'glass' in the nomenclature. Color refers of course to the color degrees of freedom of gluons. see [2]. At high energies or small distances, the gluon distribution in a hadron or nucleus becomes dense, reaching saturation.

In the CGC, gluons carry high color charge densities and form strong color fields. These fields interact with partons from the other colliding hadron or nucleus, leading to the production of a dense system of quarks and gluons known as the Glasma (gluon plasma). Instead of describing the final states by a superposition of a collection of partons in the form of

$$|qg\rangle\,, |qqg\rangle\,, \ldots, |q\bar{q}, \ldots, g, \ldots\rangle\,,$$

this final state is described by an effective field $\mathcal{A}$, and the interaction of one of the partons with the final states would be replaced by an interaction with this classical field.

In order to probe this phenomenon, a study of di-jets collisions is used. A computation of what we call the nuclear modification factor and its apparent suppression stands as a witness to this process. Studies as in [4], have utilized this framework to compute gluon distributions which will be used to assess the validity of this model. But, first we need to solve the BK equations, which is the subject of the next section.

# 3
# THE BK EQUATION

## 3.1 Theoretical formalism

The **Balitsky-Kovchegov (BK) equation** is a nonlinear evolution equation in the QCD that describes the evolution of the gluon density inside a hadron at high energy, or equivalently, at small values of Bjorken-x. It is particularly important in the study of the saturation regime, where the density of gluons becomes so high that their recombination effects become non-negligible.

The Balitsky-Kovchegov equation with running coupling constant can be written as

$$\frac{\partial N(\vec{r},y)}{\partial y} = \int d^2\vec{r_1} K(\vec{r},\vec{r_1}) \left[N(\vec{r_1},y) + N(\vec{r_2},y) - N(\vec{r},y) - N(\vec{r_1},y)N(\vec{r_2},y)\right], \tag{10}$$

where

- $y$ is the rapidity and is related to the Bjorken-x via the formula $y = \ln \frac{x_0}{x}$, where $x_0$ is taken to be equal to 0.01.
- $N(\vec{r},y)$ is the dipole scattering amplitude for a dipole of size $r$ at rapidity $y$ and is the Fourier tranform of the gluons trasnverse momentum dependence distributions that will be trated explicitely later on.
- $\vec{r_1}$ and $\vec{r_2}$ are the sizes of the two dipoles produced by the splitting of the original dipole, with $\vec{r_2} = \vec{r} - \vec{r_1}$. The vector is 2d as we have a non zero transverse momentum $k_T$.
- $K(\vec{r},\vec{r_1})$ is the evolution kernel which includes the running of the strong coupling constant $\alpha_s$, which will be chosen as

$$K(\vec{r},\vec{r_1}) = \frac{N_c\alpha_s}{2\pi^2}\frac{r^2}{r_1^2 \times (r_1^2 + r^2 - 2rr_1\cos(\theta))} \tag{11}$$

  where $\theta$ is the angle between the vectors $\vec{r}$ and $\vec{r_1}$, and $N_c$ is the number of colors.
- The terms inside the brackets represent the gain and loss terms due to gluon emissions and recombinations, accounting for saturation effects.

The specific form of the kernel $K$ and the running of the coupling constant $\alpha_s$ can vary, reflecting different approaches to incorporating the running coupling effects into the BK equation.

The BK equation can be seen as an improvement over the linear Balitsky-Fadin-Kuraev-Lipatov (BFKL) equation by including nonlinear terms that account for **gluon recombination processes**. This modification allows the BK equation to describe the unitarization of the gluon distribution at high densities, leading to the **saturation effect**.

The BK equation is part of a broader set of equations known as the JIMWLK (Jalilian-Marian, Iancu, McLerran, Weigert, Leonidov, Kovner) hierarchy, which describes the evolution

of the color fields in a high-energy hadron. However, the BK equation offers a simpler, more tractable approach by effectively resuming the JIMWLK equations to a single equation for the evolution of the dipole scattering amplitude.

The form of the BK equation with a running coupling constant, known as the rcBK equation, is more complex than the fixed-coupling case and involves modifications to the evolution kernel to account for the scale dependence of the strong coupling $\alpha_s$ The specific form of the equation with the running coupling constant can vary depending on the scheme used for the running of $\alpha_s$ and the specific implementation of the nonlinear terms that describe gluon recombination. The first aim of this project was to resolve the rcBK equation, but due to the convergence problems we have encountered, we set $\alpha_s = 0.25$ to be a constant and not running. While the rcBK improves the quantitative predictions for processes where gluon saturation, the BK equation still offers some qualitative anticipations.

## 3.2 Numerical implementation

The aim of this part is to detail the resolution of the rcBK equation in Eq. (10), which was the most challenging part of this project as there are no already implemented numerical method to solve it.

The closest known method to solve equations of this type is `scipy.integrate.solve_ivp` that solves equations of the type

$$\frac{dy}{dt} = f(t, y), \tag{12}$$

where $t$ is a 1-D parameter, $y$ is the solution function which can take values in $\mathbb{R}^D$, and $f$ is a function from $\mathbb{R} \times \mathbb{R}^D$ to $\mathbb{R}^D$. It uses multiple algorithms like the *Euler Method* and *Runge-Kutta Method*. It also requires an initial value of $y = y_0$.
We can clearly see that our equation does not correspond in its form for the moment to a type of equations like that of Eq. (12). In fact, $N(\vec{r}, y)$, the solution function, depends also on other values of $\vec{r} = \vec{r}_1$ and it does not depend thus only on the 1D parameter $y$.

An approach that we have followed is to discretize the $\mathbb{R}^2$ space in which the vectors $\vec{r}_1$ lie. This will turn the integral in Eq. (10) into a sum over the lattice we defined.

Since the $\vec{r}$ denotes the dipole sizes, we chose a spherical symmetric lattice. Since the scattering amplitudes will depend mainly on the order of magnitude of $r$, we chose the lattice to have a logarithmic scaling in $r_1$. We will fix the possible angles to 30. Thus our lattice will look like in Fig. 5.

Instead of solving now for $N(r, y)$ for a fixed $r$, we will solve for the vector

$$|N(y)\rangle = \left(N(r^{(1)}, y), \ldots, N(r^{(n)}, y)\right), \tag{13}$$

where $n$ is the number of radial subdivisions and the $r^{(i)}$ are elements of the lattice. Our

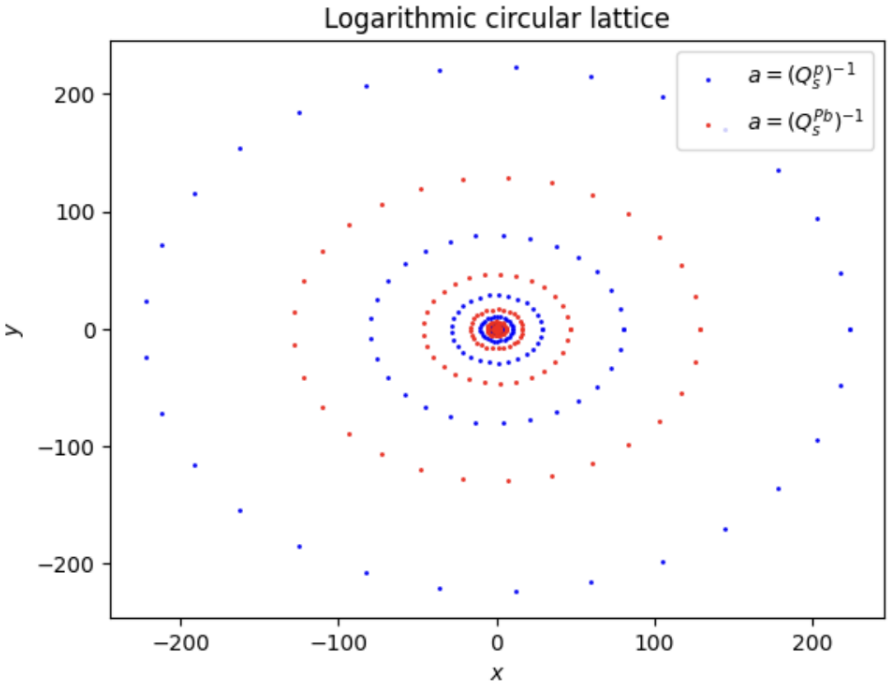


Figure 5 – Logarithmic lattice for calculating the magnetic dipole moment for both protons (in blue) and Lead (in red). The number of points along the x and y axis is $n_x = n_y = n_r = 10$, and $n_\theta = 30$.

equation will thus become

$$\frac{d}{dy}\,|N(y)\rangle = f(y, |N(y)\rangle). \tag{14}$$

This is due to the fact that $r$ and $r_1$ play a symmetrical role in the equation, thus we have the same function $f$. Determining $f$ mathematically will be a hard work since it does not serve to reduce the numerical complexity of the problem. Instead we will detail $f$ as a an algorithm.

One of the main problems is the element $N(r_2, y)$ in the integral. We have at our disposition at a single step only the elements $N(r^{(i)}, y)$. If we know the value of $N(., y)$ in $\vec{r}$ and $\vec{r_1}$, the vector $\vec{r_2} = \vec{r} - \vec{r_1}$ could or could not be in the lattice. In the latter case, we search for the closest $r^{(i)}$ and we assign its value to it. As you have seen this is not easy to define mathematically. Let's try to decompose first the integral in the Eq. (10) into smaller bits by evaluating it in the polar coordinates. The integral writes as

$$\frac{\partial N(\vec{r}, y)}{\partial y} = \int \frac{dr_1}{r_1}\left[N(r_1, y) - N(r, y)\right] \int_0^{2\pi} d\theta \frac{r^2}{r_1^2 + r^2 - 2rr_1\cos(\theta)} \tag{15}$$

$$+ \int \frac{dr_1}{r_1}\left[1 - N(r_1, y)\right] \int_0^{2\pi} d\theta \frac{r^2}{r_1^2 + r^2 - 2rr_1\cos(\theta)} N\left(\sqrt{r_1^2 + r^2 - 2rr_1\cos(\theta)}, y\right), \tag{16}$$

We also set the functions

$$g(N, r, r_1) = \int_0^{2\pi} d\theta \frac{r^2}{r_1^2 + r^2 - 2rr_1\cos(\theta)} \left[N(r_1, y) - N(r, y)\right]$$

$$h(N, r, r_1) = \int_0^{2\pi} d\theta \frac{r^2}{r_1^2 + r^2 - 2rr_1\cos(\theta)} N\left(\sqrt{r_1^2 + r^2 - 2rr_1\cos(\theta)}, y\right) \left[1 - N(r_1, y)\right]$$

The first step would be to calculate $g$ and $h$ using Simpson's rule with steps $n_\theta = 100$ and using the approximation of nearest lattice point to $r_2$.

Now that $g(N, r, r_1)$ and $h(N, r, r_1)$ are solved, we can change the variable to $\rho = \log(r)$, which will turn our equation into

$$\frac{\partial N(e^\rho, y)}{\partial y} = \int d\rho_1 g(N, e^\rho, e^{\rho_1}) + \int d\rho_1 h(N, e^\rho, e^{\rho_1}) \tag{17}$$

The judicious choice of a logarithmic $r$ scale is justified since $\rho$ follows a linear scale and thus we can use the Simpson's method to evaluate the two integrals.

Now that we can solve the Eq.(14) component by component, the only missing component is the the initial condition. The literature [1] provides us with an ansatz entitled the **McLerran-Venugopalan initial condition** which can be written

$$N_{MV}(r, y = 0) = 1 - \exp\left(-\frac{r^2 Q_{s0}^2}{4} \ln\left(\frac{1}{\Lambda_{QCD} r} + e\right)\right), \tag{18}$$

where $Q_{s0}$ is the initial saturation scale of the target which depends on the nucleon and $\Lambda_{QCD}$ is the QCD scale. This value is taken at $x = 0.01$ which correspond to $y = 0$. Per recent data, the proton has a $Q_{s0}^2(p) = 0.2GeV^2$ and the lead has a $Q_{s0}^2(Pb) = 0.6GeV^2$, which will be used. To solve the Eq. (14), we apply the Euler method. Let $dy$ be our infinitesimal displacement, $y_f$ the final value of the rapidity and $n$ the number of the steps of the algorithm to arrive at the final value. Then at the $i-$th step, we have $y_i = i \times dy$. By Euler method we have

$$|N(y_{i+1})\rangle = |N(y_i)\rangle + dy \times f(y_i, |N(y_i)\rangle) \tag{19}$$

Solving this equation yields all the values of $N(r^{(j)}, y_i)$ which enables us to plot the Dipole Scattering amplitudes dependence on $r$ at a fixed $y$, and the inverse too. The Fig. 6 shows the dependence of this function at a fixed $y$. The x-axis is plotted on a logarithmic scale to witness the exponential evolution of these amplitudes as a function of $r$. An initial remark is that the greater the rapidity $y$, the more shifted the amplitudes are along the x-axis.

A further note is that we only have a list of values of $N(., y)$, at a fixed $y$, evaluated on the lattice sites. We need a function that takes in any value of $r$ and not only on the grid. Therefore, we made a simple fit. if $r$ is inside the interval $[r_{min}, r_{max}]$, we search for the closest grid point $r_i$ to it and affect the value of $N(r_i, y)$ to it. If $r$ was big enough we use a fit $N(r) = N(r_{max})\frac{1-\exp(\ln^2(r))}{1-\exp(\ln^2(r_{max}))}$, and if it small enough we use the fit $N(r) = \frac{r^2}{r_{min}^2} N(r_{min})$.

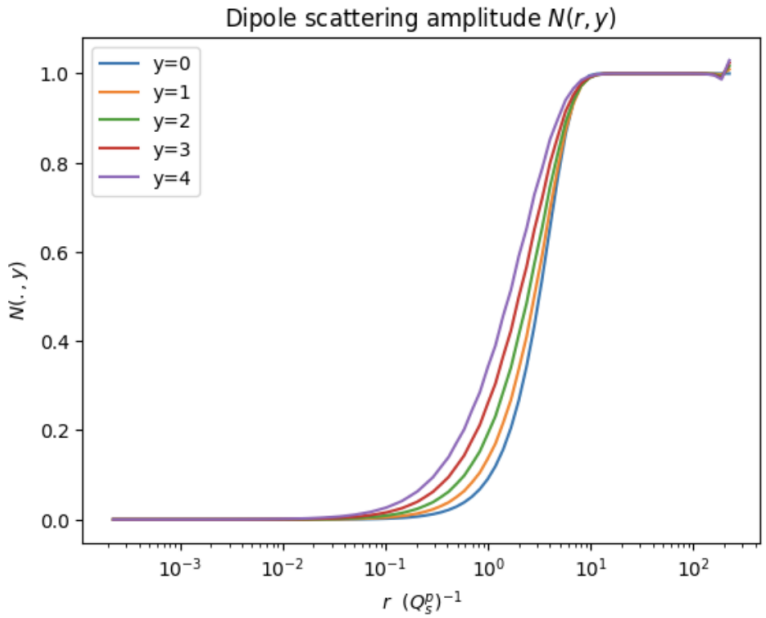


Figure 6 – Evolution of the Dipole scattering amplitude as a function of the dipole size $r$ at a fixed rapidity $y$ for the proton.

In the Fig. 6, boundary effects can be seen in the region $r \gg 1$ but do not influence the behavior of our function. From the plots we can remark slight deviations to the left as $y$ gets bigger. As predicted from the Fig.3 the saturation scale augments $Q_s$ with decreasing $x$ and thus increasing $y$. $Q_s$ can be related to the point $r$ in which the function $N(., y)$ reaches a fixed value. We can see that $r^*$ slides to the left by increasing $y$ and it can be shown that the $Q_s$ also increases correspondingly.

## 3.3 Failed attempts

Before arriving at this final result, we have made countless endeavors which were abide by failure. The plot from Fig. 1 is a result of persistence and trial-and-error. Unfortunately, I don't have the plots anymore of these attempts, since the code for the algorithm has been modified accordingly to fix the issues that will be discussed.

At the very beginning, we tried to use **Monte Carlo methods** in order to solve Eq. (10). We sample $n_s$ vectors from the disc with radius $r_{max}$ uniformly, which accounts for choosing $n_s$ $\theta$ values distributed randomly from $[0, 2\pi]$ and the square radius $r^2$ uniformly from $[0, r^2_{max}]$. The problem encountered in this method is the statistic fluctuations of the order $\frac{1}{\sqrt{n_s}}$. As we will see in the section 4, the scattering amplitude $N$, will be used to compute other distributions that will benefit us. These functions are plotted on logarithmic scale both in x-axis and y-axis. On the y-axis, they vary quickly between lower order of magnitudes that can reach even $10^{-6}$. If we want precision using MC methods, we would have needed at least $n_s = 10^12$. Computing the

convolution contributes also to the propagation of these errors from values with high standard errors to values of low standard errors. It was in this context, that we have adopted numerical integral computation algorithms like the midpoint rule.

The **midpoint rule** approximates the integral by the sum of rectangles, and we can get the hold on on the convergence. This method however has showed slight deviations from the actual values. We enhanced the precision by adopting the **Simpson's rule** which refines the rectangles into parabola-sided ones.

The story doesn't end here. We cannot give an algorithm all the mathematical ingredients and let it turn. It may or it may not converge, and even if it did, it can take a long time running which is inefficient. For this we tried to simplify the algorithm as much as possible. Instead of integrating on $(r, \theta)$ at the same time, we ran the Simpson's rule on $\theta$ to eliminate its dependence first. We were mislead by an article to choose a small number of samples $n_\theta = 25$ as it ensures convergence. It turned out that this approximation propagated some errors that manifested themselves in the long range limit ($r >> 1$) for plots of $N(r, y)$. The limit should have been exactly 1, but it deviated by an order of $10^{-2}$. It was until that we have increased the number of angle samples that the $N$'s converged to 1. The integration on $r$ was not a simple task either. We started by a linear grid, but it the algorithm showed many errors related to division by 0. For this we had to adapt the logarithmic grid and rearrange the formulas inside the integral so as not to show any `DivisionByZeroError`.

Another part was the heuristics of the sides of the integral over $r$. Theoretically, the integration should be from 0 to $\infty$ as stated before. But since we know that the function will stabilize in both sides we had to define some finite limits in order to implement computation algorithms. In the beginning, we defined the interval to be $[\frac{r_0}{100}, 100r_0]$, where $r_0 = \frac{1}{Q_{s0}}$ the inverse of the saturation scale. If we had to evaluate the amplitude on an element outside this interval, it was put into 1 or 0 depending if it is big enough or small enough respectively. But since the plots in Fig. 6 shifts to the right, this approximation could propagates, so we chose a lower bound of $\frac{r_0}{10^5}$.

Since we had to make some simplifications inside the integral, this has impeded our search for a solution to the running coupling BK equation, which was our initial intention. In this framework $\alpha_s$, the strong coupling 'constant', is not a constant but a function of $r$ proportional to $\frac{1}{\log(\Lambda r)}$. Thus also had to make some simplifications on the Kernel function $K$. in the rcBK, the kernel contains terms of $\alpha_s(r)$, but once turned into constant they vanish. This helped us to simplify the mathematics and thus the algorithmics but we restrained ourselves to BK equation solely.

# 4
# GLUON TMDS

## 4.1 Computing the gluon TMDs

The dipole scattering amplitude that we have computed in the last section $N(r,x)$ serves as a basis to compute the gluons' **Transverse Momentum Dependent (TMDs)** distributions. These functions actually describe the distribution of partons inside the proton and other hadrons with respect to both their longitudinal and transverse momenta [6]. Gluon TMDs are essential for understanding the dynamics of gluons in processes involving small-x physics, especially where gluon densities become very high, leading to phenomena such as gluon saturation.
The dipole scattering amplitude computed in the previous section will be used first to calculate different dipole gluon distributions as Fourier transforms of functions implying $N(r,y)$. Using the same notations as [5], these distributions are :

$$\mathcal{F}_{WW}(y_A,\vec{k_t}) = \frac{C_F S_L}{2\alpha_s \pi^4}\int \frac{d^2\vec{r}}{r^2} e^{-i\vec{k_t}\cdot\vec{r}}\left\{1-\left[1-N(r,y_A)\right]^2\right\}, \tag{20}$$

$$\mathcal{F}_{fund}(y_A,\vec{k_t}) = \frac{N_c k_t^2 S_L}{2\pi^2\alpha_s}\int \frac{d^2\vec{r}}{(2\pi)^2} e^{-i\vec{k_t}\cdot\vec{r}}\left[1-N(r,y_A)\right] = \frac{N_c k_t^2}{2\pi^2\alpha_s}F(y_A,k_t), \tag{21}$$

$$\mathcal{F}_{adj}(y_A,\vec{k_t}) = \frac{C_F k_t^2 S_L}{2\pi^2\alpha_s}\int \frac{d^2\vec{r}}{(2\pi)^2} e^{-i\vec{k_t}\cdot\vec{r}}\left[1-N(r,y_A)\right]^2. \tag{22}$$

$S_L$ is a constant, that represents the transverse size of target. Additional gluon TMDs are needed in the computation of the di-jet cross section Eq. (25), that will be further detailed in the next section. Thes TMDs can be obtained from the TMDs above by simple calculation, or by convolution.

$$\mathcal{F}^{(1)}_{qg}(y_A,\vec{k_t}) = \mathcal{F}_{fund}(y_A,\vec{k_t}), \tag{23a}$$

$$\mathcal{F}^{(2)}_{qg}(y_A,\vec{k_t}) = \int d^2\vec{q_t}\mathcal{F}_{WW}(y_A,\vec{q_t})F(y_A,\vec{k_t}-\vec{q_t}), \tag{23b}$$

$$\mathcal{F}^{(1)}_{gg}(y_A,\vec{k_t}) = \int d^2\vec{q_t}\mathcal{F}_{fund}(y_A,\vec{q_t})F(y_A,\vec{k_t}-\vec{q_t}), \tag{23c}$$

$$\mathcal{F}^{(2)}_{gg}(y_A,\vec{k_t}) = \mathcal{F}^{(1)}_{gg}(y_A,\vec{k_t}) - \mathcal{F}_{adj}(y_A,\vec{k_t}), \tag{23d}$$

$$\mathcal{F}^{(6)}_{gg}(y_A,\vec{k_t}) = \int d^2\vec{q_t}d^2\vec{q_t'}\mathcal{F}_{WW}(y_A,\vec{q_t})F(y_A,\vec{q_t'})F(y_A,\vec{k_t}-\vec{q_t}-\vec{q_t'}). \tag{23e}$$

We plot these TMDs for a specific value of $y_A = 4$ for the proton (Fig. 7) and for the lead (Fig. 8) as a function of the transverse momentum of the gluon $k_t$.

In gauge theories, a useful tool is to set the parameter to infinity in order to use some good approximations. In QCD, this parameter is $N_c$, the number of color charges. We know that

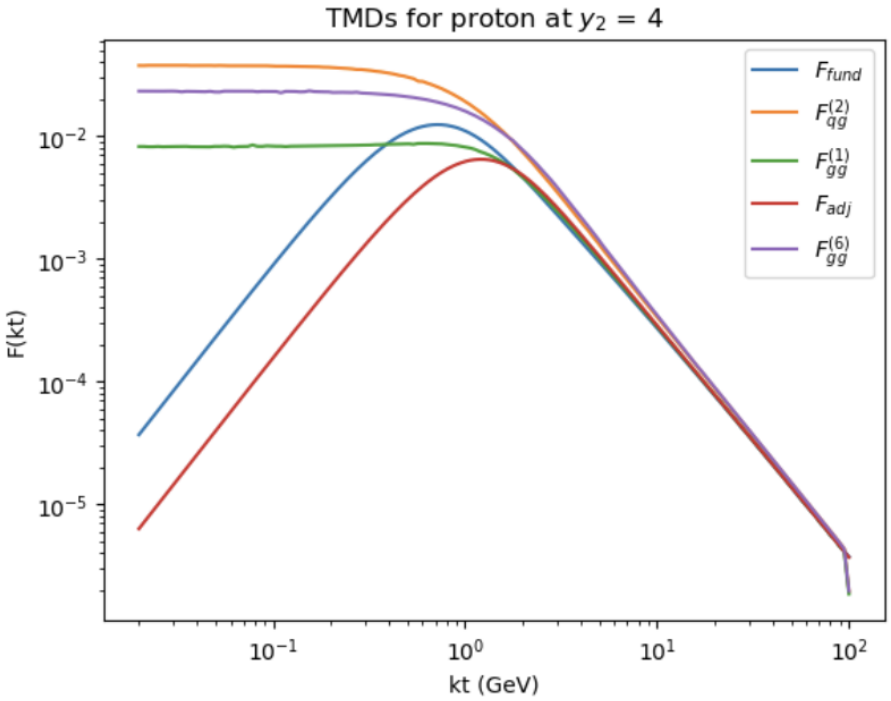


Figure 7 – The gluons TMDs for the proton at rapidity $y_A = 4$ plotted on a loglog scale as a function of the gluon momentum $k_t$ in GeV.

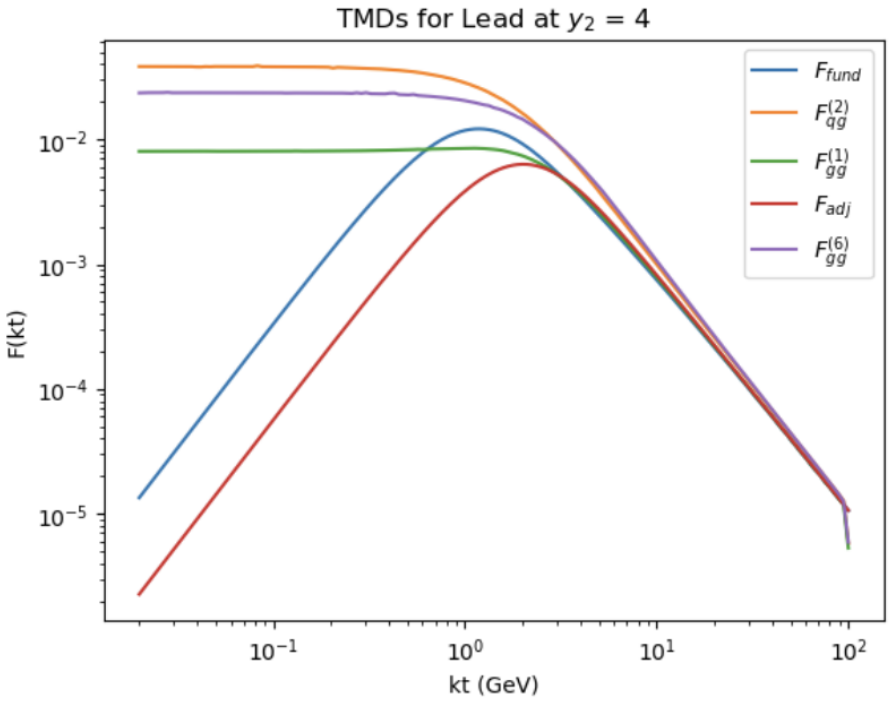


Figure 8 – The gluons TMDs for the lEAD at rapidity $y_A = 4$ plotted on a loglog scale as a function of the gluon momentum $k_t$ in GeV.

$N_c = 3$, but we chose to keep it in this format. This is t use the approximation $\frac{1}{N_c^2} = \frac{1}{9} \ll 1$. This helps us to reduce the complexity of some functions that will consist the input of a master formula in the enxt section. Furthermore, as per [5], the TMDs are imporved in the framework of CGC. We have as a result some TMDs since they are a simple linear combination of these but they take into account the initial and final states in collision. These are written as

$$\Phi^{(1)}_{qg\to qg} = F^{(1)}_{qg}, \tag{24a}$$
$$\Phi^{(1)}_{gg\to q\bar{q}} \approx F^{(1)}_{gg}, \tag{24b}$$
$$\Phi^{(1)}_{gg\to gg} \approx \frac{1}{2}\left(F^{(1)}_{gg} + F^{(6)}_{gg}\right), \tag{24c}$$
$$\Phi^{(2)}_{qg\to qg} \approx F^{(2)}_{qg}, \tag{24d}$$
$$\Phi^{(2)}_{gg\to q\bar{q}} \approx -N_c^2 F^{(2)}_{gg}, \tag{24e}$$
$$\Phi^{(2)}_{gg\to gg} \approx F^{(2)}_{gg} + F^{(6)}_{gg}. \tag{24f}$$

## 4.2 Calculation attempts

We have obtained the values of dipole scattering amplitudes numerically which works perfectly well. All that was left is to calulate the Fourier transform in 2D for a combination of these values of N.
A first attempt was to use Monte Carlo but again showed statistical fluctuation due to the term $e^{ikr}$ and the non cancellation of the imaginary parts, which has led us to complexe TMDs. Using numerical integration might have solved the problem of keeping the integral real, but it also fails to provide an accurate answer.
We used thus the function `numpy.fft.fft2` which uses the logarithmic grid to calculate the 2d Fourier transform of our functions of N.

# 5 CROSS-SECTION

## 5.1 Cross section for dijet events

The TMDs we have calculated in the previous section serve a nobel role. They are used to calculate the **cross-section** of a collision. This latter can be thought of as the probability of an event occurring when comparing it with other cross sections in the same conditions. In our particular case, we study the dijet collision and as cited in [5], the cross section for the collision in Eq. (2) is

$$\frac{d\sigma^{pA\to j_1 j_2+X}}{d^2P_t d^2k_t dy_1 dy_2} = \frac{\alpha_s^2}{(x_1x_2s)^2}\sum_{a,c,d} x_1 f_{a/p}(x_1)\sum_i \frac{1}{1+\delta_{cd}} K^{(i)}_{ag^*\to cd}(P_t,k_t)\Phi^{(i)}_{ag\to cd}(x_2,k_t), \tag{25}$$

where $\alpha_s$ is the strong coupling constant. The equation expresses the cross-section in terms of the transverse momenta $P_t, k_t$, the rapidities $y_1, y_2$, the parton distribution functions $f_{a/p}(x_1)$, the hard scattering kernels $K^{(i)}_{ag^*\to cd}$, and the gluon TMDs $\Phi^{(i)}_{ag}$. The Kronecker delta $\delta_{cd}$ accounts for symmetrization with respect to identical particles in the final state.

All of the work so far had as an end to compute the TMDs $\Phi_{ag\to cd}$. The only left component to compute the full cross section are the hard factors $K^{(i)}_{ag\to cd}$ which can be found in [4].

## 5.2 Nuclear Modification Factor

The **Nuclear Modification Factor**, often denoted as $R_{pA}$, is a quantitative measure used in high-energy nuclear physics to study the behavior of quark-gluon plasma (QGP) and other nuclear matter under extreme conditions, such as those created in nucleus-proton ($A$-$p$) collisions at facilities like the Large Hadron Collider (LHC) and the Relativistic Heavy Ion Collider (RHIC). The factor is instrumental in understanding the properties of the medium produced in such collisions, including the phenomenon of jet quenching and the modification of particle yields due to the presence of the dense and hot medium.

As cited in [3], $R_{pA}$ is defined as the ratio of the yield of particles produced in a nucleus-proton collision to the yield expected from proton-proton collisions scaled by the number of binary nucleon-nucleon collisions ($N_{coll}$) at the same energy. This scaling is necessary to account for the geometric size and density of the colliding ions and to isolate effects stemming from the dense nuclear medium itself rather than just from the increased number of nucleon-nucleon interactions. The formula for $R_{pA}$ can be expressed as :

$$R_{pA} = \frac{1}{A}\cdot\frac{d\sigma^{p+A}}{d\sigma^{p+p}},$$

where :
— $d\sigma^{p+A}$ is the differential cross-section of a given particle species in the nucleus-proton ($A$-$p$).
— $d\sigma^{p+p}$ is the differential cross-section of a given particle species in the proton-proton collision
— $A$ is the mass number for the nucleus $A$.

$R_{pA}$ can take many values, but we distinguish the following regions of values :
- $R_{pA} = 1$ : indicates that the particle production in nucleus-proton collisions is consistent with scaled-up proton-proton collisions, suggesting no nuclear medium effects.
- $R_{pA} > 1$ suggests enhancement of particle production in nucleus-proton collisions, which could be due to various nuclear effects not present in proton-proton interactions.
- $R_{pA} < 1$ indicates suppression of particle production, a signature often associated with the presence of a quark-gluon plasma where partons lose energy through interactions with the dense medium (jet quenching) and in our case a sign of CGC.

By studying $R_{pA}$ across different particle species, transverse momenta, and rapidity intervals, physicists aim to uncover the properties of the QGP and understand the complex interactions between quarks and gluons under extreme conditions.

Using the calculated TMDs $\Phi$, we have the plot Fig.9 that shows the evolution of the nuclear modifcation factor as a function of the angle $\Delta\phi$ between the two jets. Some approximations are made to the plots. We fix the pdf $x_1 f_{a/p}(x_1)$ to be equal to 1 at $x_1$ as if we know for sure the Bjorken of the incoming particle. We also fix the values of the rapidities $y_1$ and $y_2$ as well as the norm of the transverse momenta $p_{t1}$ and $p_{t2}$. The results would've been good if we had knowledge of the pdfs and if the cross sections are integrated over a range of values of rapidities and transverse momenta. Still, we can make some inference from the plot. If the jets are separated by an angle $\Delta\Phi < 3$, the factor $R_{pA}$ is almost one, meaning that there are no nuclear medium effects. However when the jets are back-to-back ($\Delta\phi \approx \pi$ we see that this factor drop below 1. In the framework of CGC this suggests some nuclear interactions related to low x-regime. Indeed, in the detectors the signature to find this form of color glass condensate is to look at the distributions of the jets produced. We remark up to an uncertainty a recession in the number of back-to-back jets which infer the existence of this form of matter.

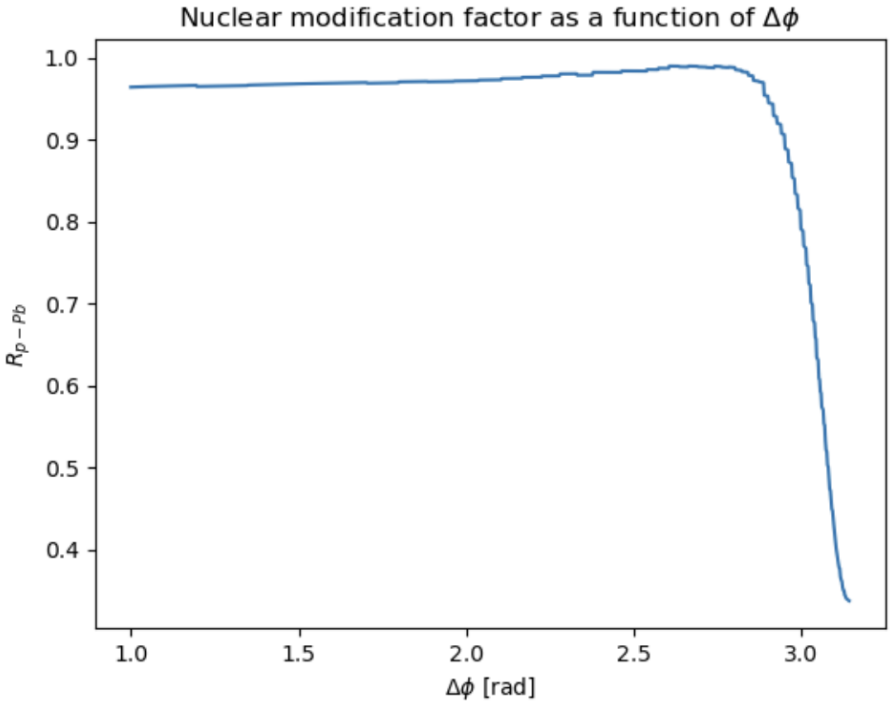


Figure 9 – The approximate Nuclear modification factor for proton-Lead as a function of $\Delta\phi$ for $y_1 = y_2 = 4$ and $p_{t1} = p_{t2} = 20GeV$.

# 6 CONCLUSION

As a conclusion, we have computed the nuclear modification factor for dilute-dense events with di-jets in the forward region in rapidity, in order to probe saturation effects for $p + Pb$ collisions. We have solved the BK equation that describes the saturation effects of gluons due to their converging effect of recombination and splitting. This helped us to compute gluon TMDs in the CGC framework and finally calculate the nuclear modification factor which shows a suppresion in the limit where the dijets are back-to-back $\Delta\phi = \pi$

# ACKNOWLEDGMENTS

I would like to thank first Mr. **Cyrille Marquet** from CPHT for accepting to supervise me on this PRL. His knowledge and expertise in QCD has helped me overcome many problems that I have faced in this project, while fueling me with a desire to delve into the world of QCD. I would also like to thank Mr. **Guilhem Gallot** and Mr. **Christophe de La Taille** for accepting my proposal to undergo a second PRL and for their trust.

# RÉFÉRENCES


[1] Larry McLerran et Raju Venugopalan. « Computing quark and gluon distribution functions for very large nuclei ». In : *Phys. Rev. D* 49 (5 mars 1994), p. 2233-2241. DOI : 10.1103/PhysRevD.49.2233. URL : https://link.aps.org/doi/10.1103/PhysRevD.49.2233.

[2] Francois Gelis et al. « The Color Glass Condensate ». In : *Ann. Rev. Nucl. Part. Sci.* 60 (2010), p. 463-489. DOI : 10.1146/annurev.nucl.010909.083629. arXiv : 1002.0333 [hep-ph].

[3] C. A. Salgado et al. « Proton-Nucleus Collisions at the LHC : Scientific Opportunities and Requirements ». In : *J. Phys. G* 39 (2012), p. 015010. DOI : 10.1088/0954-3899/39/1/015010. arXiv : 1105.3919 [hep-ph].

[4] P. Kotko et al. « Improved TMD factorization for forward dijet production in dilute-dense hadronic collisions ». In : *JHEP* 09 (2015), p. 106. DOI : 10.1007/JHEP09(2015)106. arXiv : 1503.03421 [hep-ph].

[5] A. van Hameren et al. « Forward di-jet production in p+Pb collisions in the small-x improved TMD factorization framework ». In : *JHEP* 12 (2016). [Erratum : JHEP 02, 158 (2019)], p. 034. DOI : 10.1007/JHEP12(2016)034. arXiv : 1607.03121 [hep-ph].

[6] Renaud Boussarie et al. « TMD Handbook ». In : (avr. 2023). arXiv : 2304.03302 [hep-ph].